Extracellular vesicles from blood plasma: determination of their morphology, size, phenotype and concentration.

Nicolas Arraud, Romain Linares, Sisareuth Tan, Céline Gounou, Jean-Max Pasquet, Stéphane Mornet, Alain R. Brisson

Extracellular vesicles from blood plasma: determination of their morphology, size, phenotype and concentration

N. ARRAUD,* R. LINARES,* S. TAN,* C. GOUNOU,* J.-M. PASQUET,† S. MORNET‡ and A. R. BRISSON*

**Imagerie Moléculaire et NanoBioTechnologie, UMR-5248-CBMN CNRS-University of Bordeaux-IPB, Pessac; †Hématopoïèse Leucémique et Cibles Thérapeutiques, UMR-U1035, INSERM-University of Bordeaux, Bordeaux; and ‡Chimie des Nanomatériaux, UPR-9048 ICMCB, CNRS, Pessac, France*

Summary. *Background:* Plasma and other body fluids contain membranous extracellular vesicles (EVs), which are considered to derive from activated or apoptotic cells. EVs participate in physiological and pathological processes and have potential applications in diagnostics or therapeutics. Knowledge on EVs is, however, limited, mainly due to their sub-micrometer size and to intrinsic limitations in methods applied for their characterization. *Objectives:* Our aim was to provide a comprehensive description of EVs from plasma of healthy subjects. *Methods:* Cryo-transmission electron microscopy combined with receptor-specific gold labeling was used to reveal the morphology, size and phenotype of EVs. An original approach based on sedimentation on electron microscopy grids was developed for enumerating EVs. A correlation was performed between conventional flow cytometry and electron microscopy results. *Results:* We show that platelet-free plasma samples contain spherical EVs, 30 nm to 1 μm in diameter, tubular EVs, 1–5 μm long, and membrane fragments, 1–8 μm large. We show that only a minority of EVs expose the procoagulant lipid phosphatidylserine, in contrast to the classical theory of EV formation. In addition, the concentrations of the main EV sub-populations are determined after sedimentation on EM grids. Finally, we show that conventional flow cytometry, the main method of EV characterization, detects only about 1% of them. *Conclusion:* This study brings novel insights on EVs from normal plasma and provides a reference for further studies of EVs in disease situations.

Correspondence: Alain R. Brisson, UMR-5248-CBMN, Bat. B14, Allée Geoffroy Saint-Hilaire, F-33600 Pessac, France.
Tel.: +33 5 4000 6861; fax: +33 5 4000 2200.
E-mail: a.brisson@cbmn.u-bordeaux.fr

Keywords: blood plasma; cell-derived microparticles; cryo-electron microscopy; flow cytometry; immunogold techniques.

Introduction

Cells respond to a variety of stimuli by releasing membrane vesicles, which are found in blood and other body fluids [1–4]. Two main types of cell-derived vesicles are commonly distinguished depending on their mechanism of formation and their size, namely the microparticles that originate from cell plasma membranes and range in size from 100 nm to 1 μm, and the exosomes that originate from multivesicular endosomes and are smaller, from 50 to 100 nm [3,4]. Here, the term extracellular vesicle (EV) is used for designating all types of sub-cellular particles in plasma that are surrounded by a lipid membrane bilayer [5].

Considered initially as cellular debris or waste particles [6,7], there is now increasing evidence that EVs contribute to many aspects of health and disease [8,9]. In blood, EVs participate in physiological processes of coagulation and inflammation via the presence at their surface of phosphatidylserine (PS), tissue factor and other bioactive molecules [10–12]. In addition, elevated levels of EVs of vascular origin have been found in numerous pathological disorders [13–15], including cardiovascular diseases, cancer, sepsis and autoimmune diseases [16–19]. Intense research focuses on a better understanding of the mechanisms of EV formation and on their physiopathological roles, as well as on the development of biomedical applications as disease biomarkers, drug delivery vehicles or vaccines [20–24].

Despite a wealth of methods applied for their characterization [25–27], current knowledge on EVs is scarce, so that basic questions concerning their morphology, size, phenotype or concentration remain to be elucidated. This lack of knowledge is mainly due to the sub-micrometer

size of EVs [28] and to intrinsic limitations in methods of characterization [25].

The aim of this study was to provide a comprehensive description of EVs from plasma of healthy subjects. We used cryo-transmission electron microscopy (cryo-EM), which preserves membranes in a close to native state [29], to reveal the morphology and size of EVs, and cryo-EM combined with receptor-specific gold labeling to phenotype selected EV sub-populations. This strategy was applied to pure, unprocessed plasma, in order to minimize artefactual EV formation [30,31]. In addition, a reliable approach was developed for enumerating EVs after sedimentation on EM grids. Finally, plasma samples were analyzed by flow cytometry (FCM), the main method of EV analysis [32,33], in order to determine which EVs revealed by EM are detected by FCM.

Methods

Antibodies

Anti-CD235a (glycophorin-A) and CD41 (α_{IIb} chain of $\alpha_{IIb}\beta_3$ integrin) monoclonal antibodies (mAb) were from Beckman Coulter (Villepinte, France) and Abcam (Cambridge, UK), respectively.

Preparation of plasma samples

Blood was collected after written informed consent from five healthy male donors who had fasted for at least 12 h [34]. Platelet-free plasma (PFP) was prepared within <1 h after blood collection by two cycles of centrifugation at 2500 $\times g$ for 15 min [31], as described in Data S1.

Platelet free plasma labeling with protein-conjugated gold nanoparticles

Annexin-5 gold nanoparticles (Anx5-gold-NPs) of either 4 or 10 nm diameter were produced as previously described [35]. Anti-CD235a and anti-CD41 mAbs were conjugated to 10-nm gold NPs as described in Data S1.

For Anx5 labeling, 7 μL fresh PFP were mixed with 1 μL 100 μM PPACK, 1 μL Anx5-gold-NP at 1–3 $\times$ 10^{16} NP L^{-1} and 1 μL 100 mM $CaCl_2$, incubated for 15 min at ambient temperature, then processed for cryo-EM. The same procedure was applied for anti-CD235a- and anti-CD41-gold-NP labeling, except that PPACK and $CaCl_2$ were omitted and the incubation time was 30 min. For double labeling experiments, PFP samples were labeled first with mAb-conjugated gold-NPs then with Anx5-gold-NPs.

Cryo-EM and image recording

The preparation of cryo-EM samples was started <4 h after PFP preparation. A 4-μL sample aliquot was deposited onto an EM grid coated with a perforated carbon film (Ted Pella, Redding, CA, USA), the excess liquid was blotted off with a filter paper, and the grid was then quickly plunged into liquid ethane using a Leica EM-CPC cryo-chamber. EM grids were stored in cryo-boxes under liquid nitrogen until use, then mounted in a Gatan 626 cryo-holder and transferred in a Tecnai F20 microscope operated at 200 kV. Images were recorded with an USC1000-SSCCD Gatan camera.

Values of EV size, relative amounts and concentrations are expressed as mean ± standard deviation (SD), when relevant.

Sedimentation of PFP samples over EM grids

PFP samples were labeled with Anx5-, anti-CD235a- or anti-CD41-gold-NPs, then diluted 25× with cacodylate buffer and deposited into centrifuge tubes containing four EM grids coated with a continuous carbon film fixed on a resin support (Data S1; Fig. S1). Samples were centrifuged at 100 000 $\times g$ for 1 h at 20 °C, then the liquid above EM grids was discarded, and EM grids were recovered and air dried.

Flow cytometry

Labeling of PFP samples with Anx5-fluorescein (Anx5-Fluo) or/and anti-CD235a-Cy5 mAb, as well as negative controls, is described in Data S1. FCM was performed on a Cytomics FC500 (Beckman Coulter) running CXP software version 2.2. The detection of EVs was triggered on the forward scatter (FS) parameter, and only EVs labeled with either Anx5-Fluo (FL1) or anti-CD235a-Cy5 (FL4) were taken into consideration (Data S1). EV concentrations, expressed as mean ± SD, were calculated by taking into account the flow rate, acquisition time and sample dilution.

Results

Cryo-EM reveals the morphology and size of EVs in pure plasma

Three types of EVs were distinguished on a morphological basis in pure, unprocessed PFP samples by cryo-EM (Fig. 1).

EVs presenting a circular shape in projection, hence a spherical shape in solution and named hereafter spherical EVs, constituted about half of the EVs (Fig. 1A,B). These particles are named membrane vesicles because they are limited by a lipid membrane, as evidenced by the presence at their periphery of two dark lines about 4 nm apart, which is a characteristic feature of lipid bilayers by cryo-EM [36]. Spherical EVs ranged in diameter from 30 nm to 1 μm, about 80% of them being between 50 and 500 nm (Fig. 1C).

Fig. 1. Cryo-EM of EVs from pure plasma. (A, B) Spherical EVs embedded in a thin film of frozen PFP. EV diameters are 185 nm in (A) and 45 nm and 60 nm in (B). The lipid bilayer at the periphery of EVs is resolved in two dark lines 4 nm apart (arrow in A). The granular aspect of the background is due to the high protein content of plasma. Scale bars: 100 nm. (C) Size histogram determined over 300 spherical EVs, from 30 EM grids prepared from 15 different PFP samples. The 300 images were randomly separated into three sets of 100 images; a size histogram was calculated for each set; error bars correspond to SD between the three histograms. A systematic procedure was applied for EM grid analysis. Grids were scanned first at ×300 magnification over several hundred squares for the detection of large EVs, then at ×5000 magnification for the detection of sub-μm EVs. (D) Tubular EV of 3.7 μm length and 150 nm average width. For clarity, the carbon net has been painted in light blue. The tube is suspended over the carbon net and is deformed at contact points (arrows). Scale bar: 0.5 μm. (E, F) Two examples of large fragments observed in normal PFP. (E) Elongated EV containing some internal vesicular material (arrow). Scale bar: 200 nm. (F) Large membrane fragment, of 6.5 × 7.5 μm overall size, with rounded edges. For clarity, the EV has been contoured by a white dashed line. Scale bar: 1 μm. White asterisks in A, B, D and E point to areas of the supporting carbon net.

EVs with a tubular morphology constituted also about half of the EVs observed by cryo-EM (Fig. 1D). The term tube is given to objects presenting a ratio between length and width larger than 5. The length of tubular EVs ranged from 600 nm to over 5 μm (2.2 ± 1.3 μm, $n = 100$), while their width ranged from 40 to 500 nm. Tubular vesicles appeared suspended over the supporting carbon net, presenting deformations at contact points with the carbon threads (arrows in Fig. 1D), as expected for soft objects.

The third type of EVs consisted of objects ranging in size from 1 to 8 μm, which were neither circular nor tubular, and are called hereafter large fragments (Fig. 1E,F). They represented about 10% of all EVs. About 30% of them formed a group of objects with an almost circular shape and an overall size of 6 to 8 μm (Fig. 1F).

The relative amount of spherical EVs, tubular EVs and large fragments was 50 ± 25%, 50 ± 25% and 10 ± 5%, as determined over 500 EV images recorded from 50 PFP samples. Large variations in these values were observed between EM grids, as discussed below.

Blood platelets were observed on extremely rare occasions in PFP samples (Fig. S2). They presented homogenously distributed organelles and no pseudopod extension, which is characteristic of non-activated platelets [37,38]. This indicates that the procedures applied from blood collection to cryo-EM preparation do not induce platelet activation, and therefore that the various types of EVs observed in PFP do not originate from artefactually activated cells.

In addition, small particles of 10–50 nm size not surrounded by a lipid bilayer were also observed in plasma samples, which most likely consisted of protein or lipoprotein complexes (data not shown).

Identification and characterization of PS-exposing EVs

Next, we focused on the sub-population of EVs that expose the procoagulant phospholipid PS. PS-exposing EVs are of particular interest because, according to the classical theory of EV formation at cells' plasma membranes, the loss of phospholipid asymmetry with exposure of PS molecules on the outer membrane leaflet is an early step of cell activation processes that precedes membrane blebbing and shedding of EVs [10,39,40]. Most studies on plasmatic EVs are in agreement with this theory and consider implicitly that PS-exposing EVs represent the majority, or even the totality, of EVs [26,31,41–43].

In order to label PS-exposing EVs, gold-NPs were conjugated covalently with Anx5 [35], a high-affinity ligand of PS-exposing membranes [44]. EV labeling with Anx5-gold-NPs was highly specific (Fig. 2). About half of the spherical EVs were densely covered with Anx5-gold-NPs, while the other half were unlabeled (Fig. 2A–D). Most of the tubular EVs were not labeled by Anx5. The finding that only a minority of EVs are labeled by Anx5-gold-NPs is in marked contrast to the classical theory of EV formation. Finally, we found that all the large fragments of 6–8 μm size were labeled by Anx5-gold-NPs, with no exception (Fig. 2F,G). These images demonstrate that EVs covering the whole range of size and membrane curvature can be labeled by Anx5, from small (< 100 nm) and highly curved EVs (Fig. 2C) to large (> 6 μm), almost flat, membrane fragments (Fig. 2G). No labeling was observed in the absence of $CaCl_2$, as expected from the strict Ca^{2+}-dependency of Anx5 binding to PS-exposing membranes [45].

Extracellular vesicle phenotyping by immuno-gold labeling

Next, EVs derived from erythrocytes (Ery-EVs) and platelets (PLT-EVs), the two largest blood cell populations, were characterized by immuno-gold labeling, using gold-NPs conjugated with mAbs raised against CD235a and CD41, respectively.

About 20% of spherical EVs and 30% of tubular EVs were labeled with anti- CD235a-gold-NPs (Fig. 3A,B; Fig. 4). Strikingly, all the 6–8 μm fragments were labeled with anti-CD235a-gold-NPs (Fig. 3C). When PFP samples were labeled with both 4-nm Anx5-gold-NPs and 10-nm anti-CD235a-gold-NPs, all the 6–8-μm membrane fragments were double labeled, establishing that they are of erythrocyte origin and expose PS (Fig. 3D). In view of their phenotype and size, which is the size of intact erythrocytes, we concluded that the 6–8-μm membrane fragments were empty erythrocytes and call them Ery-ghosts hereafter. Conversely, we found that (almost) none of the

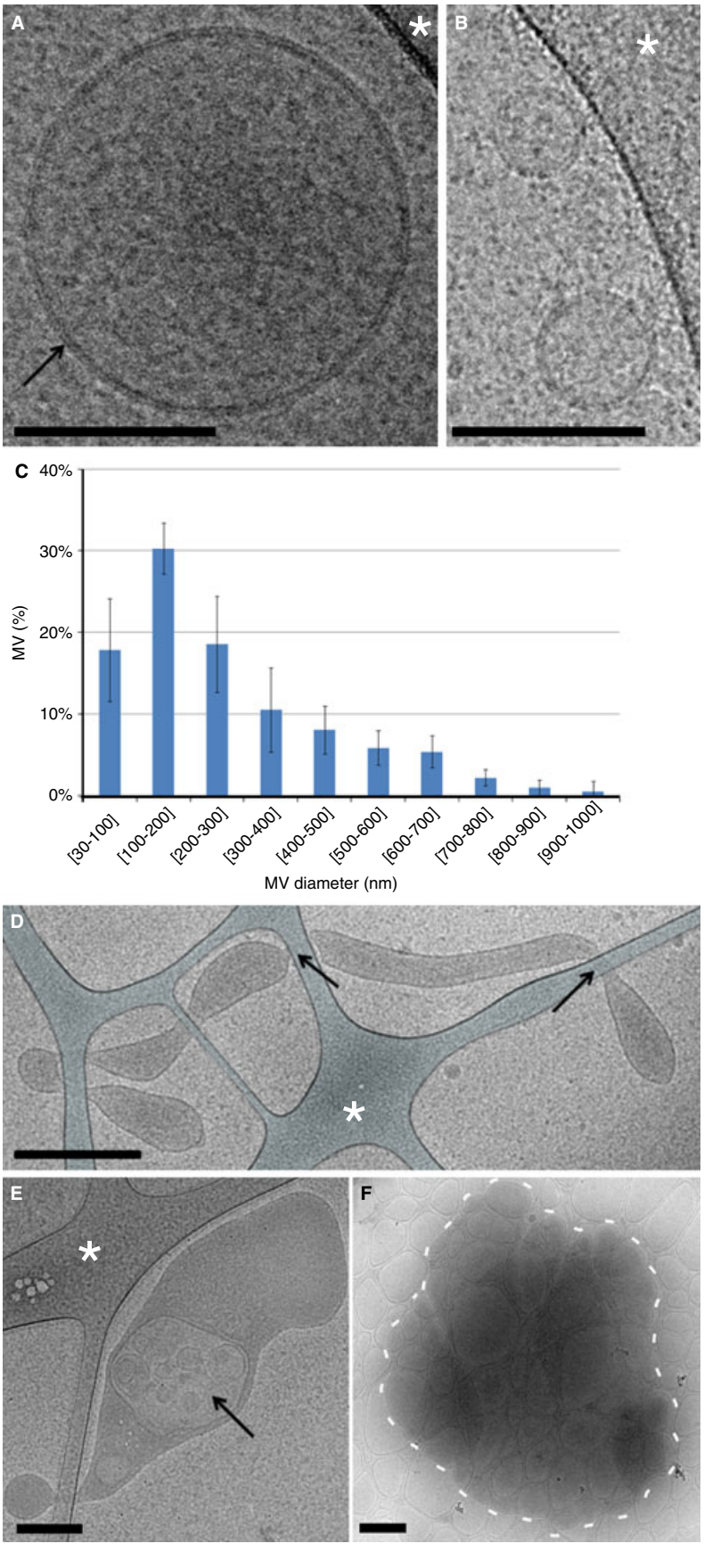
A
B
C
40%
30%
20%
10%
0%
MV (%)
[30-100]
[100-200]
[200-300]
[300-400]
[400-500]
[500-600]
[600-700]
[700-800]
[800-900]
[900-1000]
MV diameter (nm)
D
E
F

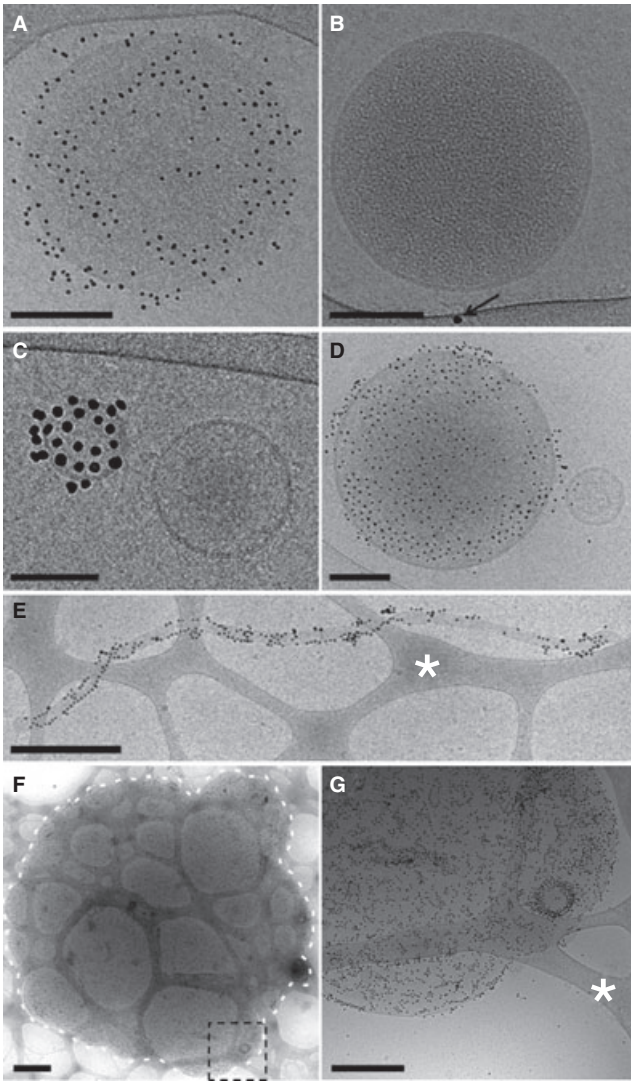

Fig. 2. Labeling of PS-exposing EVs with Anx5-gold-NPs. (A–D) Examples of spherical EVs after labeling with Anx5-gold-NPs. Some EVs are densely covered with gold-NPs (A, C, D) while other EVs are not labeled (B, C, D), demonstrating the high specificity of Anx5 labeling. Gold-NPs of 4-nm diameter were used in (A) and (D) and 10-nm diameter in (B) and (C). In (B) the arrow points to a gold-NP adsorbed on the carbon film. The concentration of gold-NPs used in this study was adjusted to give a strong labeling signal together with a minimal background signal, so that the number of gold-NPs bound per EV does not correspond to saturation and should not be taken into consideration. Scale bars: 100 nm. (E) Tubular EV of 3 μm length and 60 nm width, homogenously labeled with Anx5-gold-NPs. Only a few tubular EVs, about 10% of the total, expose PS and are labeled with Anx5-gold-NPs. Scale bar: 0.5 μm. (F, G) Large membrane fragment (F) of 8.6 μm overall width, and (G) enlarged view of the boxed area from (F). The entire surface of the membrane fragment is homogenously labeled with Anx5-gold-NPs. Scale bars: (F), 1 μm; (G), 0.5 μm. White asterisks in E and G point to areas of the carbon net.

spherical or tubular Ery-EVs were labeled with Anx5-gold-NPs, which indicates that they do not derive from Ery-ghosts, and that they are not formed by the same process as Ery-ghosts.

In view of the unexpected finding of the presence of Ery-ghosts in PFP samples, we performed complementary experiments with erythrocytes lyzed *in vitro* by osmotic shock. These experiments demonstrated that erythrocyte ghosts produced *in vitro* are identical in size and shape to Ery-ghosts from PFP samples, and also that 100% of them exposed PS, in accordance with Schrier *et al.* [46] (Fig. S3). Complementary experiments by fluorescence microscopy confirmed that the native size of *in vitro* lyzed erythrocytes was about 7 μm (Fig. S4).

Labeling PFP samples with anti-CD41-gold-NPs showed that about 30% of EVs were CD41-positive, consisting of similar proportions of spherical EVs (Fig. 3E), tubular EVs (Fig. 3F) and large fragments (Fig. 4). When PFP samples were double labeled with Anx5- and anti-CD41-gold-NPs, less than half of the CD41-positive EVs were found to expose PS (Fig. 3G). The CD41-positive/PS-negative EVs, as well as the CD235-positive/PS-negative EVs mentioned above, must therefore originate from cell plasma membranes via a mechanism in which the membrane lipid asymmetry is maintained.

Attempts to identify EVs derived from leukocytes and endothelial cells led to unsatisfactory results until now, either due to their low level in normal plasma [47] or to an inappropriate choice of antigens.

During this study, a group of tubular EVs was identified, and characterized by the absence of labeling with Anx5-, anti-CD235a- or anti-CD41-gold-NPs, and also by the presence of striations, corresponding probably to internal protein fibers (Fig. 3H,I). These triple-negative tubular EVs of yet unknown cell origin were as frequent as tubular Ery-EVs, accounting for about 30% of all tubes (Fig. 4).

Enumeration of EVs by sedimentation on EM grids

Next, we attempted to determine the absolute concentrations of EVs in normal plasma. As indicated above, the relative amounts of the three morphological types of EVs observed by cryo-EM presented large variations between samples, and also between EM grids from a given sample. We hypothesized that these variations were due to a bias in the way EVs are drained through the perforated carbon net covering cryo-EM grids. Our hypothesis was that EVs larger than the carbon net openings, like tubular EVs or large fragments, have a high probability of being retained by the net, while spherical EVs, which are smaller, are likely to pass freely through the net (Fig. S5). Consequently, the enumeration of EVs by cryo-EM would be affected by a systematic error, called 'fish-net' artifact hereafter, causing an over-estimation of the proportion of large EVs.

To overcome this problem, we developed a simple approach that consisted of sedimenting EVs by high-speed centrifugation on EM grids covered with a

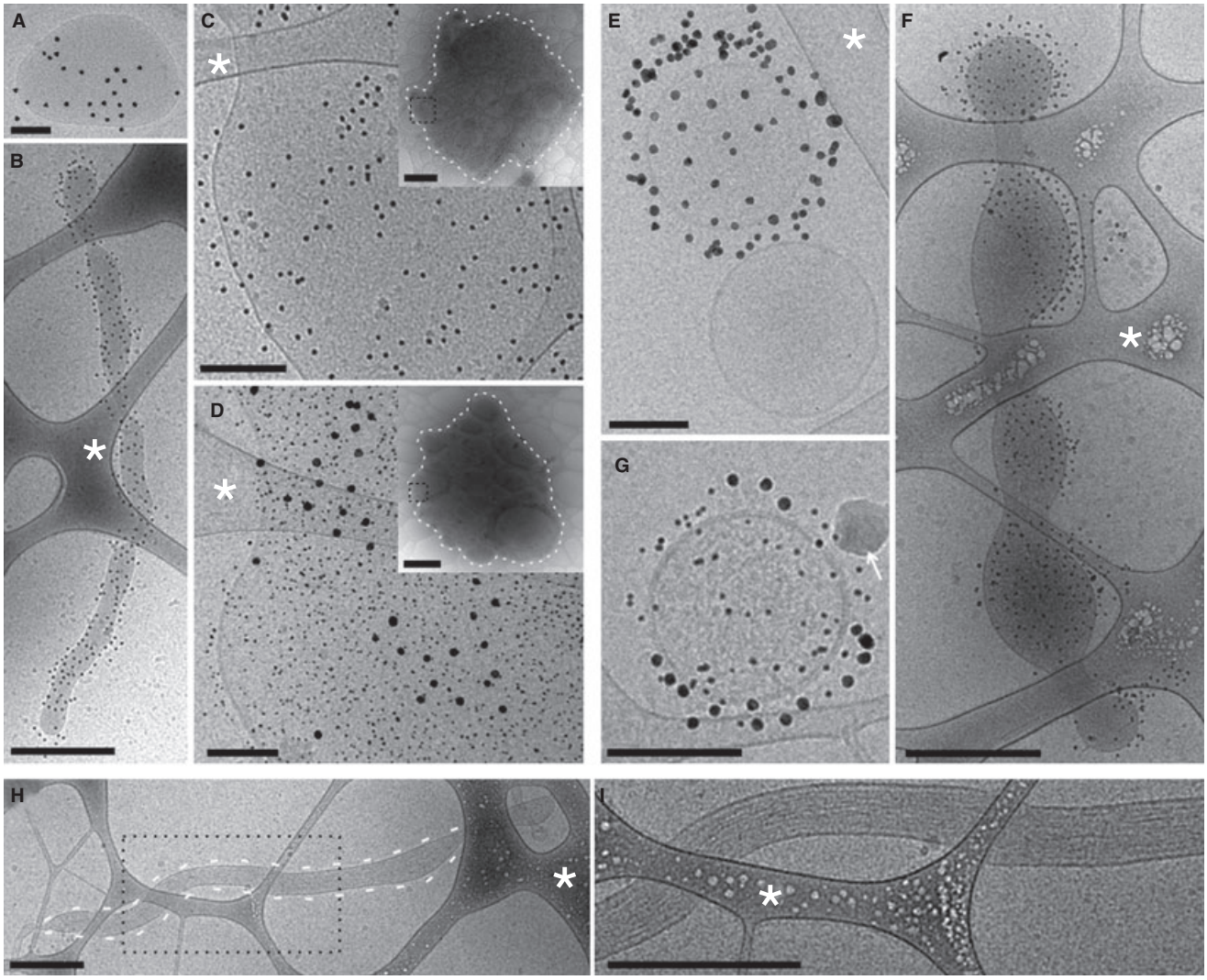

Fig. 3. Phenotyping of EVs by immuno-gold labeling. (A–D) Ery-EVs labeled with anti-CD235a-gold-NPs. (A) Ery-EV presenting an oval shape (about 450 × 300 nm). Scale bar: 100 nm. (B) Tubular EV, 4 μm long and 140 nm wide. Scale bar: 0.5 μm. (C) (inset), low magnification view of a large membrane fragment of 6 μm overall size, contoured with a white dashed line. The image represents an enlarged view of the boxed area in the inset, showing the dense and homogenous labeling with anti-CD235a-gold-NPs. Scale bar: 200 nm. (D) (inset), low magnification view of a large membrane fragment of 8.75 × 7 μm overall size, contoured with a white dashed line. The image represents an enlarged view of the boxed area in the inset, showing the double labeling with 4-nm Anx5-gold-NPs and 10-nm anti-CD235a-gold-NPs. Note the significantly higher number of Anx5-gold-NPs compared with anti-CD235a-gold-NPs, which indicates qualitatively that the number of PS binding sites is higher than the number of CD235a molecules on the membrane surface. Scale bar: 100 nm. (E–G) PLT-EVs labeled with anti-CD41-gold-NPs. (E) Two spherical EVs, one labeled with anti-CD41-gold-NPs (top), the other unlabeled (bottom), which underlines the high specificity of labeling. Most spherical CD41-positive EVs range in size between 100 and 500 nm. Scale bar: 100 nm. (F) Tubular PLT-EV, of 2.6 μm length and 360 nm width, labeled with anti-CD41-gold-NPs. Scale bar: 0.5 μm. (G) Spherical PLT-EV of 150 nm diameter double-labeled with 4-nm Anx5-gold-NPs and 10-nm anti-CD41-gold-NPs. The localization of the anti-CD41-gold-NPs at the periphery of the EV is due to a redistribution of the particles resulting from membrane flattening. The white arrow points to a contaminating ice crystal. Scale bar: 100 nm. (H, I) Tubular EVs of unknown phenotype. Example of a tubular EV that is non labeled by Anx5-, anti-CD235a- and anti-CD41-gold-NPs. For clarity, the tube has been contoured with a white dashed line in (H). (I) Enlarged view of the boxed area in (H) revealing longitudinal striations, which are likely to correspond to internal protein fibers. Scale bars: 0.5 μm. White asterisks (B–F, H–I) point to areas of the supporting carbon net.

continuous carbon film, and then quantifying EVs by EM after air-drying (Fig. S1). The high salt and protein content of plasma make specimens prepared in this way almost non-amenable to EM analysis. However, when PFP samples were labeled with protein-conjugated gold-NPs prior to sedimentation, EVs could be clearly identified due to their homogenous and high-density decoration with gold-NPs (Fig. 5A–E).

The validity of this approach was first evaluated with suspensions of *in vitro* prepared erythrocyte ghosts of known concentrations. We found that 75 ± 15% (n = 3) of the actual amount of erythrocyte ghosts was recovered

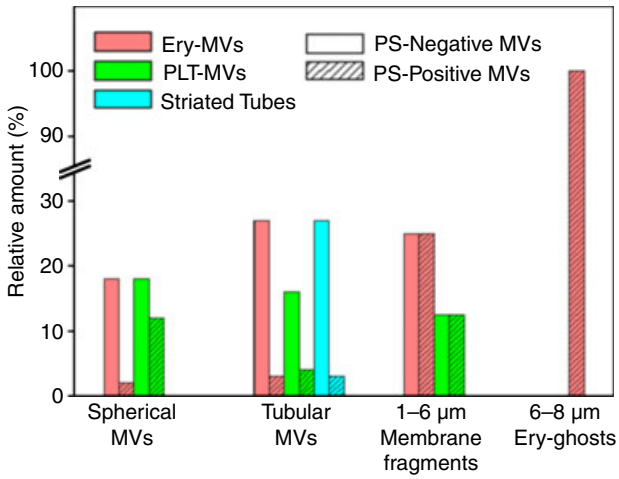

Fig. 4. Relative amounts of the different EV sub-populations determined by cryo-EM. The percentages of PS-negative (plain color) and PS-positive (dashed color) Ery-EVs (pink) and PLT-EVs (green) are represented for the three morphological families. In addition, the percentages of PS-negative and PS-positive EVs are represented for the sub-population of striated tubular EVs (blue), considered here as a 'negative' phenotype, because these EVs are CD235a negative and CD41 negative. The morphological family of large fragments has been divided into two groups, because the 6–8-µm Ery-ghosts constitute a group of unique origin.

on EM grids after sedimentation. This result was considered satisfactory, validating the sedimentation approach for quantifying EVs, at least for large objects such as erythrocyte ghosts. On the other hand, attempts to identify control particles for sub-µm EVs have as yet been unsuccessful.

The procedure was then applied to PFP samples, starting with the quantification of Ery-ghosts, which are easily recognizable due to their characteristic shape and strong labeling with Anx5-gold-NPs (Fig. 5D,E). The absolute concentration of Ery-ghosts was found to be 60 ± 30 µL^{-1} pure PFP. To quantify the other types of EVs, a stringent method of counting was applied, in which only the objects that presented a high and homogenous gold-NP labeling with a well-defined near-to-circular or tubular shape were taken into account. EVs were found to range in size from 80 nm to 8 µm (Fig. 5F). About 95% of EVs were smaller than 1 µm, with a diameter of 275 ± 150 nm. Considering that a sphere flattens into a disk upon sedimentation, the corresponding sphere would have a diameter of about 200 nm. Table 1 gives the concentrations determined for the various EV sub-populations. Overall, the number of spherical EVs was about 20 times larger than that of tubular EVs, and more than 200 times larger than that of large fragments. This validates the 'fish-net' artefact hypothesis presented above. It is likely that the concentration of EVs smaller than about 100 nm was under-estimated in this analysis, due to their weaker labeling and possible shape alterations induced by sedimentation and/or air-drying.

In addition, these experiments showed that the number of residual platelets in PFP samples was < 1 platelet µL^{-1}.

Correlation between FCM and EM

Finally, PFP samples were characterized by FCM, the main method used in EV studies [32,33], in order to find out which EV populations identified by EM were detected by FCM. In these FCM experiments, the trigger was set on the forward scatter (FS) parameter and the detection was limited to fluorescently labeled EVs, following standard procedures [31] (Fig. 6, Fig. S6). The concentration of Anx5-positive EVs was found to be 500 ± 190 ($n = 18$) µL^{-1} pure PFP, consistent with previous reports [30,31,42]. Consequently, when we compare this value with the concentration of Anx5-positive EVs determined by the sedimentation approach, about 30 000 µL^{-1}, we must conclude that conventional FCM detects about 1% of the EVs.

Guided by our EM results, we attempted to identify the Ery-ghosts by FCM, assuming that they would form a distinct population due to their large size. A cluster of highly fluorescent EVs was indeed identified in single labeling experiments with either Anx5-Fluo (Fig. 6A,B) or anti-CD235a-Cy5 (Fig. 6C,D), as well as in double labeling experiments (Fig. 6E,F). This cluster of events must therefore correspond to Ery-ghosts. We must stress that the presence of a well-identified cluster of Ery-ghosts was observed by FCM with each PFP sample investigated during this study. With the pre-analytical conditions used here, the concentration of Ery-ghosts in PFP was 145 ± 80 EVs µL^{-1} ($n = 18$). This value is close to the concentration determined by the sedimentation approach, about 60 Ery-ghosts µL^{-1}, providing further evidence of the reliability of the sedimentation approach.

A striking result of this study was that 6–8 µm Ery-ghosts present light scattering properties similar to 500-nm polystyrene beads with our flow cytometer

Fig. 5. EVs sedimented on EM grids after receptor-specific gold labeling. (A, B) Spherical EVs labeled with Anx5-gold-NPs. These EVs are called spherical by extension of our cryo-EM observations, even though their shape may be distorted due to sedimentation and/or air-drying. Scale bars: (A) 200 nm; (B) 500 nm. (C) Tubular EV labeled with anti-CD235a-gold-NPs. The tube appears dark, most likely due to the presence of hemoglobin. Scale bar: 1 µm. (D, E) Ery-ghost, 7 µm in overall size, labeled with Anx5-gold-NPs. In (D) the Ery-ghost has been contoured with a white dashed line. (E) Enlarged view of the red boxed area in (D). Ery-ghosts are the easiest EVs to recognize after sedimentation on EM grids due to their characteristic size and their high density labeling with either Anx5- or anti-CD235a-gold-NPs. Scale bar: 1 µm. (F) Size histogram of all EVs, determined over 500 images of EVs recorded on three EM grids. Error bars correspond to SD between the three individual datasets.

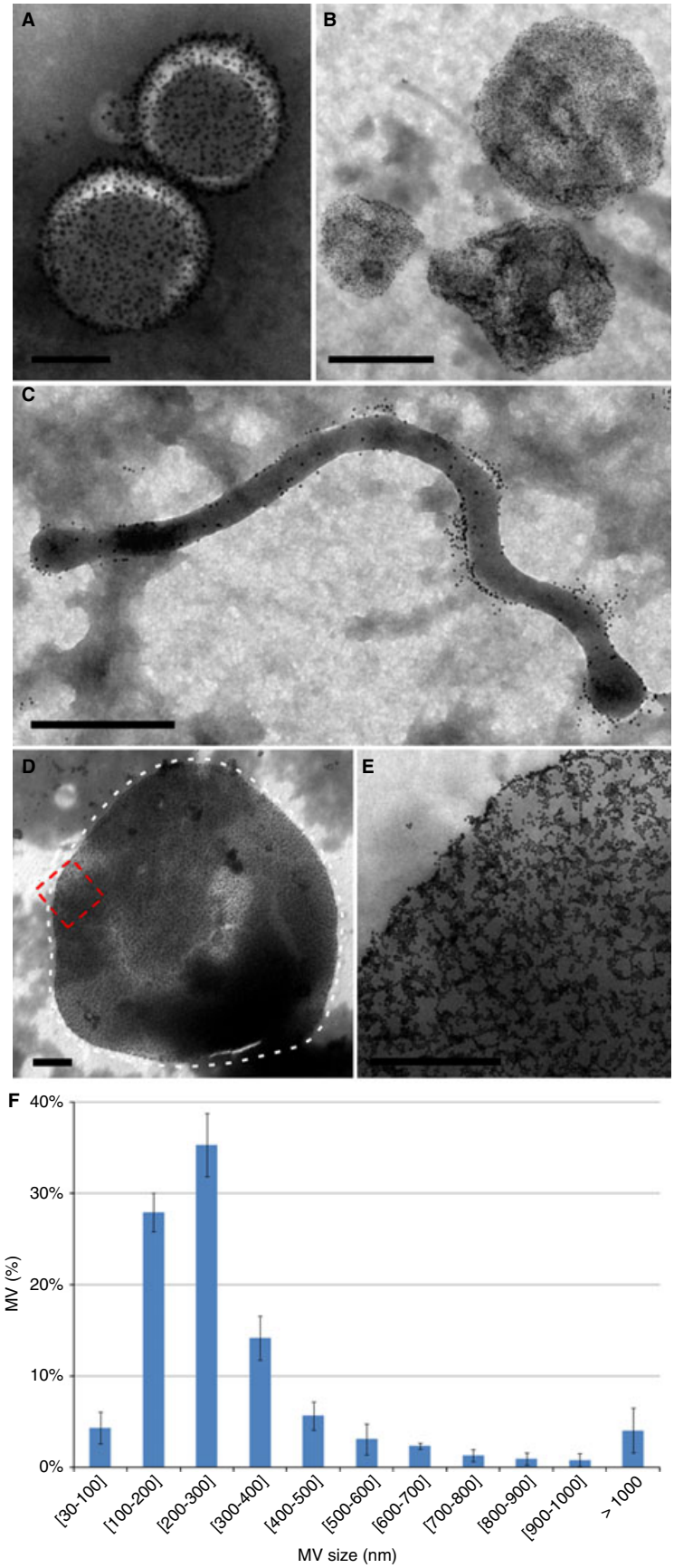
A
B
C
D
E
F
40%
30%
20%
10%
0%
MV (%)
[30-100]
[100-200]
[200-300]
[300-400]
[400-500]
[500-600]
[600-700]
[700-800]
[800-900]
[900-1000]
> 1000
MV size (nm)

Table 1 Concentrations of EVs in PFP determined by sedimentation on EM grids

			Large fragments	
	Spherical EVs*	Tubular EVs	1–6 μm	Ery-ghosts 6–8 μm
PS-positive EVs	**28 000 ± 7000**	220 ± 100	ND	**60 ± 30**
Ery-EVs	2600 ± 600	**1800 ± 800**	ND	**60 ± 30**
PLT-EVs	11 500 ± 5500	220 ± 100	ND	0
All EVs	**> 95%**	**< 5%**	**< 0.5%**	

PS-positive EVs, Ery-EVs and PLT-EVs were identified by labeling with Anx5-, anti-CD235a- and anti-CD41-gold-NPs, respectively.
The PS-positive spherical EVs*, tubular Ery-EVs and Ery-ghosts are the most easily recognizable EVs. They are marked in bold here to indicate that their corresponding concentrations are more reliable.
To calculate EV concentrations, the numbers of EVs were counted over at least 100 EM grid squares for Ery-ghosts and at least five grid squares for spherical and tubular EVs. The numbers of EVs per grid square (of 2750 μm2 area) were converted into the total number of EVs sedimented on the entire surface of the epoxy resin support, namely 113 mm2, and then divided by the volume of pure PFP used in the sedimentation experiment, namely 150 μL, in order to obtain EV concentrations μL−1 pure PFP.
*EVs smaller than 1 μm are called spherical EVs although their shape after sedimentation may be slightly distorted.
ND, not determined.

(Fig. 6, B, D and F). In view of this unexpected result, hitherto unreported, complementary FCM experiments were performed with erythrocyte ghosts produced *in vitro*. These experiments confirmed that erythrocyte ghosts formed a cluster of events scattering light similarly to 500-nm polystyrene beads (Fig. S6G).

Discussion

This study provides novel insights on the morphology, size, phenotype and concentration of EVs from plasma of healthy donors.

We show that plasma contains spherical EVs, of about 200-nm diameter, tubular EVs, with a mean length close to 2 μm, and large fragments, 1–8 μm in size. This description is significantly different from the common view that EVs are spherical vesicles ranging in size from 50 to 500 nm, which is mainly based on EM [26,28], atomic force microscopy (AFM) [26,48,49] and nanoparticle tracking analysis (NTA) [50]. Although tubes and large fragments represent only about 5% and 0.5% of EVs, respectively, their total membrane surfaces are of the same order of magnitude as that of spherical EVs, which may be important for functions exerted via surface-exposed receptors.

Our finding that a majority of EVs are not labeled by Anx5 is in contrast to classical models of EV formation [10,43,51] and most studies on EVs which consider that the majority, or even the totality, of plasmatic EVs consist of PS-exposing EVs [26,31,41–43]. Although several FCM studies [30,52–55] have reported the presence of Anx5-negative EVs, the fact that FCM detects only a minority of EVs does not allow a direct comparison with our results. Concerning the origin of the Anx5-negative EVs, we considered two main hypotheses: (i) these EVs do not expose PS, (ii) these EVs expose PS but either Anx5 binding is prevented by the prior binding of other PS-binding proteins, or the level of PS is insufficient for Anx5 binding [56]. This second hypothesis is considered unlikely, principally because the proportion of Anx5-positive EVs was observed to increase when PFP samples were kept at 4 °C for several days or were centrifuged and resuspended, which suggests a transfer of PS molecules from the inner to the outer membrane leaflet of previously Anx5-negative EVs [57]. PS-negative EVs must therefore form via a mechanism that maintains the plasma membrane phospholipid asymmetry. We propose that tubular EVs, which are PS-negative for most of them, form by direct fragmentation of vascular cells, in a process analogous to the formation of platelets from megakaryocytes [58]. By extension, PS-negative spherical EVs may also form by cell fragmentation, or by scission of PS-negative tubes, as suggested by the observed tendency of tubes to fragment into vesicles (Fig. 7). Reininger *et al.* [59] have shown that tubular membrane tethers several tens of μm long form when platelets interact, under high shear conditions with von Willebrand factor-coated surfaces, and that increasing shear stress led to the formation of EVs. In the case of synthetic lipid tubes, it is well established that tubes submitted to various physical constraints transform into vesicles, a phenomenon known as pearling instability [60].

Fig. 6. Flow cytometry analysis of a PFP sample. (A, C, E) Ungated Anx5-Fluo (FL1) vs. anti-CD235a-Cy5 (FL4) plots. (B, D, F) Forward scatter (FS) vs. side scatter (SS) plots corresponding to A, C and E, representing events falling in gates A1 (blue), A2 (green), A4-B (red) and B (purple). The positions of 500-nm and 1-μm microbeads are indicated. (A, B) Single labeling experiment with Anx5-Fluo. All events labeled with Anx5 present FS values lower than 1-μm microbeads, as expected for PFP EVs (B). A cluster of highly fluorescent events, located in gate B (purple), is apparent in FL1 vs. FL4 plots (A). These events have FS/SS values close to those of 500-nm microbeads. (C, D) Single labeling experiment with anti-CD235a-Cy5. Events labeled with anti-CD235a-Cy5 appear as a single cluster in gate A1 (blue) (C). They present FS/SS values close to those of 500-nm microbeads (D). (E, F) Double labeling experiment with Anx5-Fluo and anti-CD235a-Cy5. A cluster of events labeled with both Anx5-Fluo and anti-CD235a-Cy5 is observed in gate A2 (green). This cluster contains most of the events previously located in gates B and A1 in single labeling experiments with Anx5-Fluo and anti-CD235a-Cy5, respectively (E). Events positive only for Anx5 are still observed in gate A4-B (red). The double labeled events present FS/SS values close to those of 500-nm microbeads (F). These results indicate that most of the events presenting a high Anx5 labeling intensity are of erythrocyte origin and therefore correspond to the Ery-ghosts identified by EM.

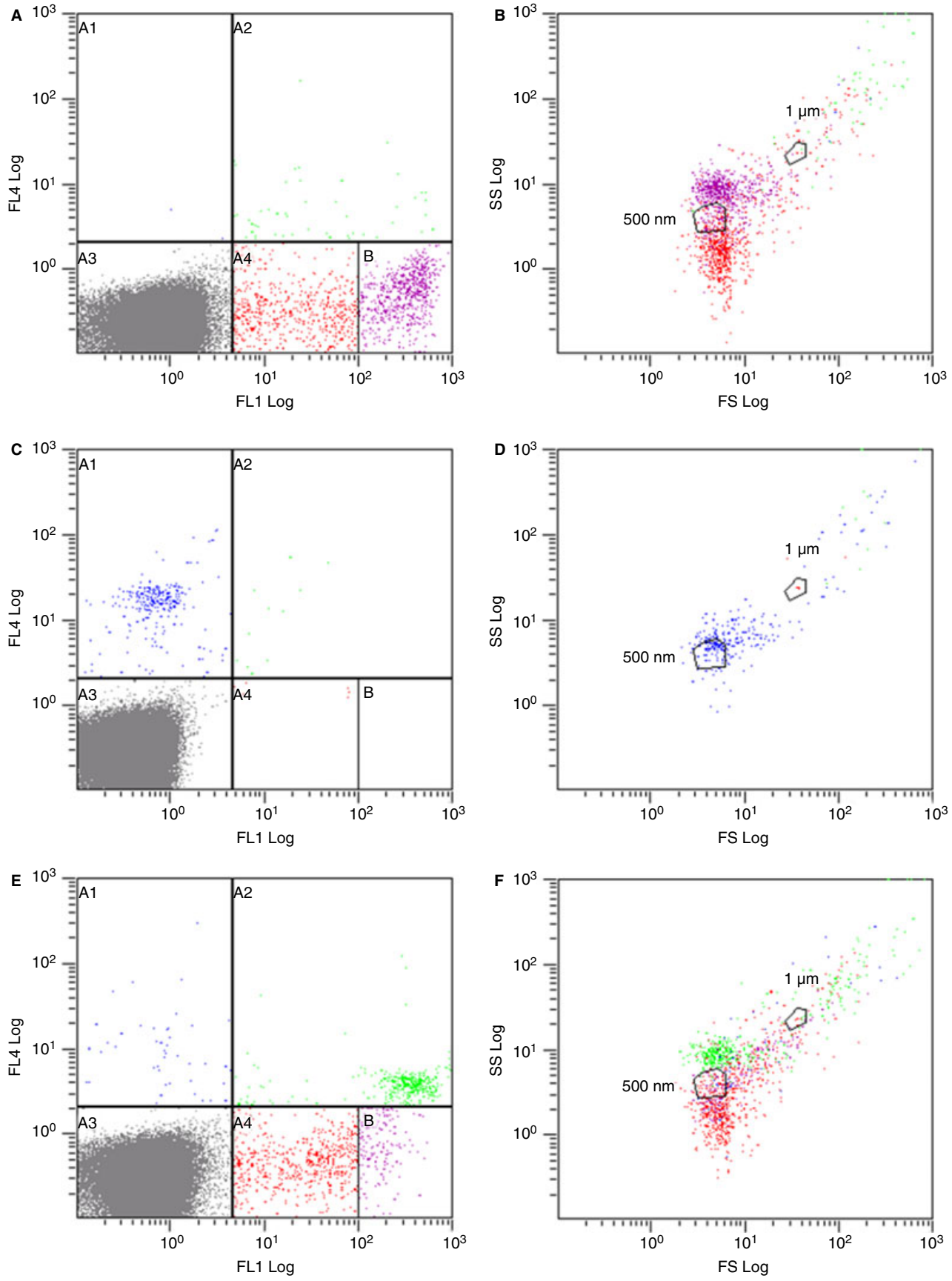
A
B
C
D
E
F
A1
A2
A3
A4
B
FL4 Log
FL1 Log
SS Log
FS Log
1 µm
500 nm
10^0
10^1
10^2
10^3

Cryo-EM and immuno-gold labeling allowed a detailed characterization of the sub-populations of Ery-EVs and PLT-EVs, showing that they account for more than 50% of all EVs. As reported by Heijnen *et al*. [28], activated platelets produce not only EVs that originate from the plasma membrane and are CD41-positive, but also exosomes originating from multi-vesicular endosomes, which are CD41-negative. Consequently, the identification of the entire population of PLT-EVs will require the use of additional markers. Further work will also be needed to characterize the sub-populations of EVs deriving from leukocytes and endothelial cells, as well as to identify the cell origin of the striated tubular EVs (Fig. 3H–I).

The unanticipated presence of Ery-ghosts in PFP samples deserves some comments. Although Ery-ghosts have not been identified until now in PFP samples, it is most likely that they account for part of Ery-EVs reported in previous FCM studies. An obvious question is whether Ery-ghosts are present in blood or are created during or after blood collection. Interestingly, the number of Ery-ghosts found in PFP is close to the number of erythrocytes that are eliminated from the circulation in several minutes [61]. Ery-ghosts may therefore correspond to the end stage of red blood cells' life. The question of the genuine existence vs. the artefactual creation of Ery-ghosts is of importance because the presence of PS molecules at their surface may confer on them a role *in vivo* in blood coagulation homeostasis [62] or *in vitro* in the properties of blood bank products [63].

By correlating EM and FCM, we found that conventional FCM detects only about 1% of EVs. In addition, we show that 6–8-μm fragments have light scattering properties comparable to 500-nm polystyrene beads. This result adds some objective information to a series of recent discussions questioning the use of polymer beads for size calibration of biological objects [25,64,65]. Although Ery-ghosts have the same size as intact erythrocytes, their FS/SS values are considerably different (Fig. S6G–H). This is certainly due to differences in refractive indices between hemoglobin-full and hemoglobin-empty erythrocytes.

The relative amounts of spherical EVs, tubular EVs and large fragments determined by the sedimentation approach are about 95%, 5% and 0.5%. We consider that the absolute concentrations of tubular EVs and large fragments are reliable because these objects are easily recognizable. On the other hand, it is likely that the concentrations of spherical EVs of small size, smaller than about 100 nm, is under-estimated, due to their weaker labeling and possible shape distortion. We estimate therefore that the relative amounts of the three morphological types of EVs are: > 95% spherical EVs, < 5% tubular EVs and < 0.5% large fragments (Table 1). At this stage of the analysis, a conservative statement is that one microliter of pure plasma contains at least 50 000 spherical EVs and 2000 tubular EVs. How do these values compare to published work? There is little agreement in the literature concerning the concentration of EVs in plasma, with values ranging from 200 to 10^9 EVs μL^{-1} [50,66]. Low EV concentrations have been consistently obtained by

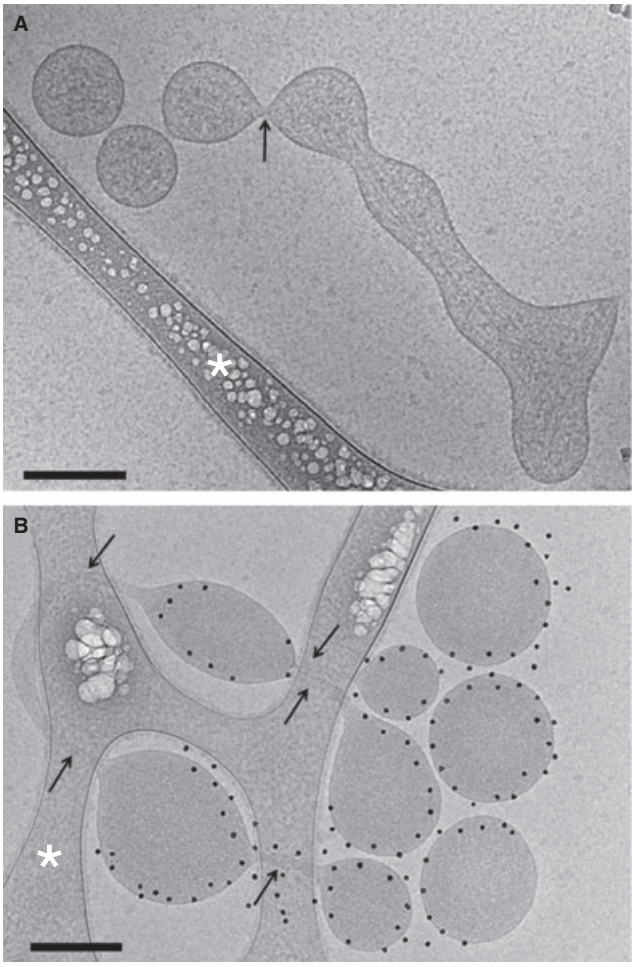

Fig. 7. Fragmentation of tubular EVs into spherical EVs. (A) Tubular EV of 1.45 μm length and 140 nm width. The upper left extremity of the tube is fragmented into three spherical EVs of about 140 nm diameter. The spherical EV closest to the tube extremity is still associated with the tubular part by a thin connecting material (arrow). Note that the diameter of the spherical EVs is close to the diameter of the tubular portion. We speculate that fragmentation resulted from mechanical constraints associated with shear effects during thin film formation. This image was recorded from a PFP sample labeled with Anx5-, anti-CD235a- and anti-CD41-gold-NPs. The lack of labeling with Anx5-gold-NPs indicates that the tube fragmentation into vesicles was not accompanied by the exposure of PS molecules. (B) Tubular Ery-EV, 2.2 μm long, labeled with anti-CD235a-gold-NPs, which has fragmented into an ensemble of spherical EVs of 220 nm average diameter. It is likely that fragmentation was induced by mechanical constraints associated with deposition of the tube on the underlying carbon net; the tube areas in direct contact with the carbon film are stretched into thin tubules (arrows), which may break below a size limit and give rise to spherical vesicles. White asterisks in A and B point to areas of the carbon net. Scale bars: 200 nm.

conventional FCM, which is in agreement with our finding that FCM detects only a minority of EVs. On the other hand, EV concentrations up to 10^9 EVs μL^{-1} PFP have been reported by NTA [50,67], hence several orders of magnitude larger than our EM results. It is likely that non-vesicular particles like lipoproteins or macromolecular complexes contribute to these large values, as shown by Dragovic *et al*. [50].

Important progress has been made recently in the EV field with the development of standardized protocols of sample preparation and of EV measurement conditions in FCM [30,33,64,68]. Further progress is expected from the development of flow cytometers with improved detection capabilities [47,64,69], or the application of novel detection strategies, such as the triggering of small particles by fluorescence in FCM [69,70]. These developments, together with improved methods of EV purification [69,71,72], sorting [73] and proteo/genomic analysis [72,74], should lead to a better knowledge and understanding of EVs' origin, composition and properties. This is critical for evaluating objectively the roles of EVs in health and disease, as well as their potential biomedical applications.

In conclusion, this work improves our basic knowledge on EVs from normal plasma. We believe it constitutes a reference for further studies of EVs in pathological situations.

Addendum

N. Arraud contributed to the supervision of the project and performed the preparation of the blood samples and the FCM studies; R. Linares and S. Tan performed the EM experiments; R. Linares and S. Mornet synthesized the protein-functionalized gold nanoparticles; C. Gounou produced the Anx5 proteins and contributed to the FCM experiments; J. M. Pasquet contributed to the initial phase of elaboration of the project; A. R. Brisson coordinated the entire project.

Acknowledgements

We thank Ms Guillonet, Ms Chaléat, Ms Tarascon and Mr Le Provost (Laboratoire Mutualiste d'Analyses Médicales de Pessac) for their help with the collection of blood samples. We thank R. Bérat for his participation at the beginning of this study and A. Bouter for his help with fluorescence microscopy experiments. We thank A. Nurden, P. Nurden and P. Bassereau for helpful discussions. This study was supported by ANR (grants EMPB-MP-NPAuA5-2007-021-01 and 11-BSV1-03501-PlacentA5 to AB).

Disclosure of Conflict of Interests

The authors state that they have no conflict of interests.

Supporting Information

Additional Supporting Information may be found in the online version of this article:

Data S1. Materials.
Fig. S1. Scheme of the procedure of EV sedimentation on EM grids.
Fig. S2. Cryo-EM image of a blood platelet in PFP.
Fig. S3. Cryo-EM image of an erythrocyte ghost produced *in vitro* by osmotic shock.
Fig. S4. Fluorescence microscopy image of *in vitro* lyzed erythrocytes.
Fig. S5. Scheme of the 'fish-net' artefact of cryo-EM analysis of PFP samples.
Fig. S6. Flow cytometry.

References

1 Théry C, Ostrowski M, Segura E. Membrane vesicles as conveyors of immune responses. *Nat Rev Immunol* 2009; **9**: 581–93.
2 György B, Szabó TG, Pásztói M, Pál Z, Misják P, Aradi B, László V, Pállinger É, Pap E, Kittel Á, Nagy G, Falus A, Buzás EI. Membrane vesicles, current state-of-the-art: emerging role of extracellular vesicles. *Cell Mol Life Sci* 2011; **68**: 2667–88.
3 van der Pol E, Böing AN, Harrison P, Sturk A, Nieuwland R. Classification, functions, and clinical relevance of extracellular vesicles. *Pharmacol Rev* 2012; **64**: 676–705.
4 Raposo G, Stoorvogel W. Extracellular vesicles: exosomes, microvesicles, and friends. *J Cell Biol* 2013; **200**: 373–83.
5 Gould SJ, Raposo G. As we wait: coping with an imperfect nomenclature for extracellular vesicles. *J Extracell Vesicles* 2013; **2**: 20389.
6 Wolf P. The nature and significance of platelet products in human plasma. *Br J Haematol* 1967; **13**: 269–88.
7 Pan BT, Teng K, Wu C, Adam M, Johnstone RM. Electron microscopic evidence for externalization of the transferrin receptor in vesicular form in sheep reticulocytes. *J Cell Biol* 1985; **101**: 942–8.
8 Valadi H, Ekström K, Bossios A, Sjöstrand M, Lee JJ, Lötvall JO. Exosome-mediated transfer of mRNAs and microRNAs is a novel mechanism of genetic exchange between cells. *Nat Cell Biol* 2007; **9**: 654–9.
9 Burger D, Schock S, Thompson CS, Montezano AC, Hakim AM, Touyz RM. Microparticles: biomarkers and beyond. *Clin Sci* 2013; **124**: 423–41.
10 Zwaal RFA, Schroit AJ. Pathophysiologic implications of membrane phospholipid asymmetry in blood cells. *Blood* 1997; **89**: 1121–32.
11 Morel O, Toti F, Hugel B, Freyssinet J-M. Cellular microparticles: a disseminated storage pool of bioactive vascular effectors. *Curr Opin Hematol* 2004; **11**: 156–64.
12 Zwicker JI, Trenor CC, Furie BC, Furie B. Tissue factor-bearing microparticles and thrombus formation. *Arterioscler Thromb Vasc Biol* 2011; **31**: 728–33.
13 Horstman LL, Ahn YS. Platelet microparticles: a wide-angle perspective1. *Crit Rev Oncol Hematol* 1999; **30**: 111–42.
14 VanWijk MJ, VanBavel E, Sturk A, Nieuwland R. Microparticles in cardiovascular diseases. *Cardiovasc Res* 2003; **59**: 277–87.
15 Morel O, Toti F, Hugel B, Bakouboula B, Camoin-Jau L, Dignat-George F, Freyssinet J-M. Procoagulant microparticles disrupting the vascular homeostasis equation? *Arterioscler Thromb Vasc Biol* 2006; **26**: 2594–604.

16 Wiedmer T, Hall SE, Ortel TL, Kane WH, Rosse WF, Sims PJ. Complement-induced vesiculation and exposure of membrane prothrombinase sites in platelets of paroxysmal nocturnal hemoglobinuria. *Blood* 1993; **82**: 1192–6.
17 Manly DA, Wang J, Glover SL, Kasthuri R, Liebman HA, Key NS, Mackman N. Increased microparticle tissue factor activity in cancer patients with Venous Thromboembolism. *Thromb Res* 2010; **125**: 511–2.
18 Boilard E, Nigrovic PA, Larabee K, Watts GFM, Coblyn JS, Weinblatt ME, Massarotti EM, Remold-O'Donnell E, Farndale RW, Ware J, Lee DM. Platelets amplify inflammation in arthritis via collagen-dependent microparticle production. *Science* 2010; **327**: 580–3.
19 Delabranche X, Boisramé-Helms J, Asfar P, Berger A, Mootien Y, Lavigne T, Grunebaum L, Lanza F, Gachet C, Freyssinet J-M, Toti F, Meziani F. Microparticles are new biomarkers of septic shock-induced disseminated intravascular coagulopathy. *Intensive Care Med* 2013; **39**: 1695–703.
20 Zitvogel L, Regnault A, Lozier A, Wolfers J, Flament C, Tenza D, Ricciardi-Castagnoli P, Raposo G, Amigorena S. Eradication of established murine tumors using a novel cell-free vaccine: dendritic cell derived exosomes. *Nat Med* 1998; **4**: 594–600.
21 Skog J, Würdinger T, van Rijn S, Meijer DH, Gainche L, Curry WT, Carter BS, Krichevsky AM, Breakefield XO. Glioblastoma microvesicles transport RNA and proteins that promote tumour growth and provide diagnostic biomarkers. *Nat Cell Biol* 2008; **10**: 1470–6.
22 Alvarez-Erviti L, Seow Y, Yin H, Betts C, Lakhal S, Wood MJA. Delivery of siRNA to the mouse brain by systemic injection of targeted exosomes. *Nat Biotechnol* 2011; **29**: 341–5.
23 Peinado H, Alečković M, Lavotshkin S, Matei I, Costa-Silva B, Moreno-Bueno G, Hergueta-Redondo M, Williams C, García-Santos G, Ghajar CM, Nitadori-Hoshino A, Hoffman C, Badal K, Garcia BA, Callahan MK, Yuan J, Martins VR, Skog J, Kaplan RN, Brady MS, *et al*. Melanoma exosomes educate bone marrow progenitor cells toward a pro-metastatic phenotype through MET. *Nat Med* 2012; **18**: 883–91.
24 Zwicker JI, Liebman HA, Bauer KA, Caughey T, Campigotto F, Rosovsky R, Mantha S, Kessler CM, Eneman J, Raghavan V, Lenz H-J, Bullock A, Buchbinder E, Neuberg D, Furie B. Prediction and prevention of thromboembolic events with enoxaparin in cancer patients with elevated tissue factor-bearing microparticles: a randomized-controlled phase II trial (the Microtec study). *Br J Haematol* 2013; **160**: 530–7.
25 van der Pol E, Hoekstra AG, Sturk A, Otto C, van Leeuwen TG, Nieuwland R. Optical and non-optical methods for detection and characterization of microparticles and exosomes. *J Thromb Haemost* 2010; **8**: 2596–607.
26 György B, Módos K, Pállinger É, Pálóczi K, Pásztói M, Misják P, Deli MA, Sipos Á, Szalai A, Voszka I, Polgár A, Tóth K, Csete M, Nagy G, Gay S, Falus A, Kittel Á, Buzás EI. Detection and isolation of cell-derived microparticles are compromised by protein complexes resulting from shared biophysical parameters. *Blood* 2011; **117**: e39–48.
27 Witwer KW, Buzás EI, Bemis LT, Bora A, Lässer C, Lötvall J, Nolte-'t Hoen EN, Piper MG, Sivaraman S, Skog J, Théry C, Wauben MH, Hochberg F. Standardization of sample collection, isolation and analysis methods in extracellular vesicle research. *J Extracell Vesicles* 2013; **2**: 20360.
28 Heijnen HFG, Schiel AE, Fijnheer R, Geuze HJ, Sixma JJ. Activated platelets release two types of membrane vesicles: microvesicles by surface shedding and exosomes derived from exocytosis of multivesicular bodies and alpha-granules. *Blood* 1999; **94**: 3791–9.
29 Dubochet J, Adrian M, Chang JJ, Homo JC, Lepault J, McDowall AW, Schultz P. Cryo-electron microscopy of vitrified specimens. *Q Rev Biophys* 1988; **21**: 129–228.
30 Ayers L, Kohler M, Harrison P, Sargent I, Dragovic R, Schaap M, Nieuwland R, Brooks SA, Ferry B. Measurement of circulating cell-derived microparticles by flow cytometry: sources of variability within the assay. *Thromb Res* 2011; **127**: 370–7.
31 Lacroix R, Judicone C, Poncelet P, Robert S, Arnaud L, Sampol J, Dignat-George F. Impact of pre-analytical parameters on the measurement of circulating microparticles: towards standardization of protocol. *J Thromb Haemost* 2012; **10**: 437–46.
32 Jy W, Horstman LL, Jimenez JJ, Ahn YS. Measuring circulating cell-derived microparticles. *J Thromb Haemost* 2004; **2**: 1842–3.
33 Robert S, Poncelet P, Lacroix R, Arnaud L, Giraudo L, Hauchard A, Sampol J, Dignat-George F. Standardization of platelet-derived microparticle counting using calibrated beads and a Cytomics FC500 routine flow cytometer: a first step towards multicenter studies? *J Thromb Haemost* 2009; **7**: 190–7.
34 Cantero M, Conejo J, Parra T, Jiménez A, Carballo F, de Arriba G. Interference of chylomicrons in analysis of platelets by flow cytometry. *Thromb Res* 1998; **91**: 49–52.
35 Brisson A, Mornet S. Functionalization of gold nanoparticles with oriented proteins. Application to the High-Density Labelling of Cell Membranes Patent WO/2007/122259, 2007.
36 Lambert O, Gerke V, Bader M-F, Porte F, Brisson A. Structural analysis of junctions formed between lipid membranes and several annexins by cryo-electron microscopy. *J Mol Biol* 1997; **272**: 42–55.
37 Morgenstern E. Human platelet morphology/ultrastructure. In: von Bruchhausen F, Walter U, eds. *Platelets and Their Factors*. Berlin Heidelberg: Springer, 1997: 27–60.
38 White JG. Chapter 3 – platelet structure. In: Alan D, Michelson MD, eds. *Platelets*, 2nd edn. Burlington: Academic Press, 2007: 45–73.
39 Bevers EM, Comfurius P, Zwaal RFA. Changes in membrane phospholipid distribution during platelet activation. *Biochim Biophys Acta* 1983; **736**: 57–66.
40 Fadok VA, Voelker DR, Campbell PA, Cohen JJ, Bratton DL, Henson PM. Exposure of phosphatidylserine on the surface of apoptotic lymphocytes triggers specific recognition and removal by macrophages. *J Immunol* 1992; **148**: 2207–16.
41 Biró E, Sturk-Maquelin KN, Vogel GMT, Meuleman DG, Smit MJ, Hack CE, Sturk A, Nieuwland R. Human cell-derived microparticles promote thrombus formation in vivo in a tissue factor-dependent manner. *J Thromb Haemost* 2003; **1**: 2561–8.
42 Aras O, Shet A, Bach RR, Hysjulien JL, Slungaard A, Hebbel RP, Escolar G, Jilma B, Key NS. Induction of microparticle- and cell-associated intravascular tissue factor in human endotoxemia. *Blood* 2004; **103**: 4545–53.
43 Morel O, Jesel L, Freyssinet J-M, Toti F. Cellular mechanisms underlying the formation of circulating microparticles. *Arterioscler Thromb Vasc Biol* 2011; **31**: 15–26.
44 Tait JF, Gibson DF, Smith C. Measurement of the affinity and cooperativity of annexin V–membrane binding under conditions of low membrane occupancy. *Anal Biochem* 2004; **329**: 112–9.
45 Andree HA, Reutelingsperger CP, Hauptmann R, Hemker HC, Hermens WT, Willems GM. Binding of vascular anticoagulant alpha (VAC α) to planar phospholipid bilayers. *J Biol Chem* 1990; **265**: 4923–8.
46 Schrier SL, Zachowski A, Hervé P, Kader J-C, Devaux PF. Transmembrane redistribution of phospholipids of the human red cell membrane during hypotonic hemolysis. *Biochim Biophys Acta* 1992; **1105**: 170–6.
47 Robert S, Lacroix R, Poncelet P, Harhouri K, Bouriche T, Judicone C, Wischhusen J, Arnaud L, Dignat-George F. High-sensitivity flow cytometry provides access to standardized measurement of small-size microparticles—brief report. *Arterioscler Thromb Vasc Biol* 2012; **32**: 1054–8.
48 Yuana Y, Oosterkamp TH, Bahatyrova S, Ashcroft B, Garcia Rodriguez P, Bertina RM, Osanto S. Atomic force microscopy:

a novel approach to the detection of nanosized blood microparticles. *J Thromb Haemost* 2010; **8**: 315–23.
49 Ashcroft BA, de Sonneville J, Yuana Y, Osanto S, Bertina R, Kuil ME, Oosterkamp TH. Determination of the size distribution of blood microparticles directly in plasma using atomic force microscopy and microfluidics. *Biomed Microdevices* 2012; **14**: 641–9.
50 Dragovic RA, Gardiner C, Brooks AS, Tannetta DS, Ferguson DJP, Hole P, Carr B, Redman CWG, Harris AL, Dobson PJ, Harrison P, Sargent IL. Sizing and phenotyping of cellular vesicles using Nanoparticle Tracking Analysis. *Nanomedicine* 2011; **7**: 780–8.
51 Record M, Carayon K, Poirot M, Silvente-Poirot S. Exosomes as new vesicular lipid transporters involved in cell-cell communication and various pathophysiologies. *Biochim Biophys Acta* 2014; **1841**: 108–20.
52 Joop K, Berckmans RJ, Nieuwland R, Berkhout J, Romijn FP, Hack CE, Sturk A. Microparticles from patients with multiple organ dysfunction syndrome and sepsis support coagulation through multiple mechanisms. *Thromb Haemost* 2001; **85**: 810–20.
53 Jimenez JJ, Jy W, Mauro LM, Horstman LL, Ahn YS. Elevated endothelial microparticles in thrombotic thrombocytopenic purpura: findings from brain and renal microvascular cell culture and patients with active disease. *Br J Haematol* 2001; **112**: 81–90.
54 Connor DE, Exner T, Ma DDF, Joseph JE. The majority of circulating platelet-derived microparticles fail to bind annexin V, lack phospholipid-dependent procoagulant activity and demonstrate greater expression of glycoprotein Ib. *Thromb Haemost* 2010; **103**: 1044–52.
55 Boulanger CM, Amabile N, Tedgui A. Circulating microparticles a potential prognostic marker for atherosclerotic vascular disease. *Hypertension* 2006; **48**: 180–6.
56 Richter RP, Lai Kee Him J, Tessier B, Tessier C, Brisson AR. On the kinetics of adsorption and two-dimensional self-assembly of annexin A5 on supported lipid bilayers. *Biophys J* 2005; **89**: 3372–85.
57 Devaux PF. Protein involvement in transmembrane lipid asymmetry. *Annu Rev Biophys Biomol Struct* 1992; **21**: 417–39.
58 Italiano JE Jr, Hartwig JH. Chapter 2 – megakaryocyte development and platelet formation. In: Alan D, Michelson MD, eds. *Platelets*, 2nd edn. Burlington: Academic Press, 2007: 23–44.
59 Reininger AJ, Heijnen HFG, Schumann H, Specht HM, Schramm W, Ruggeri ZM. Mechanism of platelet adhesion to von Willebrand factor and microparticle formation under high shear stress. *Blood* 2006; **107**: 3537–45.
60 Tsafrir I, Sagi D, Arzi T, Guedeau-Boudeville M-A, Frette V, Kandel D, Stavans J. Pearling instabilities of membrane tubes with anchored polymers. *Phys Rev Lett* 2001; **86**: 1138–41.
61 Bratosin D, Mazurier J, Tissier JP, Estaquier J, Huart JJ, Ameisen JC, Aminoff D, Montreuil J. Cellular and molecular mechanisms of senescent erythrocyte phagocytosis by macrophages. A review. *Biochimie* 1998; **80**: 173–95.
62 Whelihan MF, Mann KG. The role of the red cell membrane in thrombin generation. *Thromb Res* 2013; **131**: 377–82.
63 Simak J, Gelderman MP. Cell membrane microparticles in blood and blood products: potentially pathogenic agents and diagnostic markers. *Transfus Med Rev* 2006; **20**: 1–26.
64 Chandler WL, Yeung W, Tait JF. A new microparticle size calibration standard for use in measuring smaller microparticles using a new flow cytometer. *J Thromb Haemost* 2011; **9**: 1216–24.
65 van der Pol E, van Gemert MJC, Sturk A, Nieuwland R, van Leeuwen TG. Single vs. swarm detection of microparticles and exosomes by flow cytometry. *J Thromb Haemost* 2012; **10**: 919–30.
66 Shet AS, Aras O, Gupta K, Hass MJ, Rausch DJ, Saba N, Koopmeiners L, Key NS, Hebbel RP. Sickle blood contains tissue factor–positive microparticles derived from endothelial cells and monocytes. *Blood* 2003; **102**: 2678–83.
67 Gercel-Taylor C, Atay S, Tullis RH, Kesimer M, Taylor DD. Nanoparticle analysis of circulating cell-derived vesicles in ovarian cancer patients. *Anal Biochem* 2012; **428**: 44–53.
68 Lacroix R, Robert S, Poncelet P, Dignat-George F. Overcoming limitations of microparticle measurement by flow cytometry. *Semin Thromb Hemost* 2010; **36**: 807–18.
69 van der Vlist EJ, Nolte-'t Hoen ENM, Stoorvogel W, Arkesteijn GJA, Wauben MHM. Fluorescent labeling of nano-sized vesicles released by cells and subsequent quantitative and qualitative analysis by high-resolution flow cytometry. *Nat Protoc* 2012; **7**: 1311–26.
70 Nolan JP, Stoner SA. A trigger channel threshold artifact in nanoparticle analysis. *Cytometry A* 2013; **83A**: 301–5.
71 Eldh M, Lötvall J, Malmhäll C, Ekström K. Importance of RNA isolation methods for analysis of exosomal RNA: evaluation of different methods. *Mol Immunol* 2012; **50**: 278–86.
72 Kalra H, Adda CG, Liem M, Ang C-S, Mechler A, Simpson RJ, Hulett MD, Mathivanan S. Comparative proteomics evaluation of plasma exosome isolation techniques and assessment of the stability of exosomes in normal human blood plasma. *Proteomics* 2013; **13**: 3354–64.
73 Leong HS, Podor TJ, Manocha B, Lewis JD. Validation of flow cytometric detection of platelet microparticles and liposomes by atomic force microscopy. *J Thromb Haemost* 2011; **9**: 2466–76.
74 Noerholm M, Balaj L, Limperg T, Salehi A, Zhu LD, Hochberg FH, Breakefield XO, Carter BS, Skog J. RNA expression patterns in serum microvesicles from patients with glioblastoma multiforme and controls. *BMC Cancer* 2012; **12**: 22.